PNAS
www.pnas.org

Loss of *Arc* attenuates the behavioral and molecular responses for sleep homeostasis in mice

Ayako Suzuki, Masashi Yanagisawa, Robert W. Greene

Correspondence should be addressed to Masashi Yanagisawa, M.D., Ph.D. or Robert W. Greene, M.D., Ph.D.

Email: yanagisawa.masa.fu@u.tsukuba.ac.jp or robertw.greene@utsouthwestern.edu

This PDF file includes:

Supplementary Information Text

Materials and Methods

Animals. Eight-week-old male C57BL/6 mice (Wakeland Laboratory, UTSW) and C57BL/6-background GFP knock-in *Arc* KO mice (Ref. 1, breeding pairs kindly provided by Dr. Kimberly Huber, UTSW) were housed under a 12 h/12 h light/dark cycle. Once mice were housed individually, they were gently handled once a day until the experimental day.

Behavioral Studies. Electroencephalography (EEG) and electromyography (EMG) electrode implantation was performed as follows: anteroposterior (AP): 1.7 mm, mediolateral (ML): 1.8 mm, dorsoventral (DV): –1.3 mm; and AP: –1.7 mm, ML: 1.8 mm, DV: –1.3 mm. All mice were allowed 14 days of recovery from surgery. Subsequently, mice were tethered, transferred onto a treadmill, and allowed 3 weeks of habituation on the recording system, after which EEG/EMG signals were monitored continuously for a 48-h period. Sleep deprivation (SD) and selective REM deprivation experiments were carried out from ZT0–4 following a 24-h baseline EEG/EMG recording. The EEG/EMG signal was monitored during sleep deprivation (ZT0–4) and recovery sleep (ZT4–24). 4-h total SD was conducted using a treadmill at a speed of 1.0 m/min. REM SD was achieved by gentle handling under real-time EEG/EMG monitoring after REM sleep (theta wave) for 5 s continuously. Selective REM deprivation was performed gently, to allow mice to resume NREM sleep within 5 s after REM sleep disturbance via gentle handling. The REM sleep signal was detected as a combination of EEG wave amplitude reduction and EMG atonia. NREM delta energy was calculated as the averaged delta power (μV^2) multiplied by NREM sleep duration (min) over 2 h. Δ NREM delta energy was subtracted values of 4-h SD NREM delta energy from that of baseline at each matching time points. The scoring and analysis were performed using MatLab (MathWorks), as described previously (2).

Nonbehavioral studies. Mouse brains without EEG/EMG implantation were used in all nonbehavioral studies. Mice were randomly assigned into four treatment groups; *ad libitum* sleep (control) at ZT4, and ZT6, 4 h SD (SD), and 2 h recovery sleep after 4 h SD (recovery). All brain samples were collected at ZT4 (control or SD) or ZT6 (control or recovery sleep).

Antibodies. All primary [anti-Arc (Santa Cruz Biotechnology, catalog #: sc-17839), anti-GluA1 (Santa Cruz Biotechnology, catalog #: sc-55509), anti-GluR1 Ser^{831} (Phosphosolutions, catalog #: p1160-831), anti-GluR1 Ser^{845} (Phosphosolutions, catalog #: p1160-845), anti-lamin B (Proteintech, catalog #: 12987-1-AP), anti-beta tubulin (Cell Signaling Technology, catalog #: 2146), anti-histone H3 (Cell Signaling Technology, catalog #: 4499), and anti-GAPDH (Cell Signaling Technology, catalog #: 5174)] and secondary [anti-mouse IgG–HRP (Santa Cruz Biotechnology, catalog #: sc-2005), anti-rabbit IgG–HRP (Santa Cruz Biotechnology, catalog #: sc-2357), and anti-mouse IgG–Alexa 594 (Molecular Probes, catalog #: A-11032)] antibodies were commercially obtained.

SDS–PAGE and Immunoblotting. Protein samples were separated using appropriate concentrations of acrylamide SDS–PAGE and transferred onto PVDF membranes. After antibody incubations, target protein signals were detected using the SuperSignal West Pico Chemiluminescence Substrate (Thermo Scientific) or the ECL™ Prime Western Blotting Detection System (GE Healthcare). Membranes were used repeatedly after stripping.

Coomassie Staining. The membrane was briefly washed with a fixing solution (50% methanol and 10% acetic acid), incubated with a staining solution (fixing solution containing 0.1% Coomassie Brilliant Blue R-250), and washed with the fixing solution until signals reached the desired staining levels for detection. For

immunoblot analysis, three bands were collected: >75 kDa, between 48–75 kDa, and <48 kDa, respectively, and the densitometry values of each band were combined in individual mice and then averaged. These values were used for the normalization of immunoblots of synaptoneurosomal samples (3).

Synaptoneurosome Preparation. As described in SI Ref. 4, mice were deprived of total sleep for 4 h and synaptoneurosomes from the frontal cortex were prepared. Subsequently, synaptoneurosomes were lysed in 2.5% SDS, boiled for 10 min, and a 50-μg aliquot was used as synaptoneurosome sample. A total homogenate that was filtrated through a 100-μm membrane was combined with an adequate amount of 10% SDS solution to the final concentration of 1% SDS. Synaptoneurosome protein was validated by immunoblot (Fig. S3) using samples of total homogenate, synaptoneurosome, and supernatant.

RNA Extraction, Reverse Transcription PCR, and Quantitative Real-Time PCR (qRT–PCR). Total RNA was extracted from the frontal cortex sample and reverse transcribed to cDNA, as described in SI Ref. 4. qRT–PCR was carried out using the primer pairs listed in SI Applendix, Table S1 under 30 PCR cycles. All reactions were normalized to *GAPDH*, which was used as an endogenous control, and expressed relatively.

Immunofluorescence. For immunofluorescence, brains were perfused with PBS and 4% paraformaldehyde in PBS, immersed in 30% sucrose in PBS for 48 h at 4° C, and sectioned into 35-μm slices using a microtome. A free-floating method was used in this experiment. Coronal brain sections were washed with PBS three times, blocked and permeabilized with 2% blocking solution (Roche) in PBS containing 0.3% Triton X-100 for 1 h at room temperature, and incubated with the primary antibody overnight at 4° C, followed by the anti-mouse Alexa 568 antibody for 2 h at room temperature. Excess amounts of antibodies were washed out with PBS after antibody incubation. DAPI was used for the detection of nuclei (ProLong Gold Antifade Reagent, Invitrogen).

Cell Counting. Cell counts for nuclear Arc-positive cells and subcellular localization were made in the layer II-IV of the motor cortex area (bregma ± 100 μm) from two to three consecutive sections per mouse. Prior to cell counting, fluorescence images obtained with an Olympus BX-60 microscope (60x objective) were adjusted using Adobe Photoshop CS5. The following output/input levels were used: Red, 0-153/36-115; Blue, 0-140/26-133; Green, entirely off. These threshold values were obtained according to the pixel intensities for nuclear Arc staining in SD samples. Then, cell counting was done blindly in all four conditions. Cells were counted (150–200 cells per brain; 10–15 brains in each condition) using images adjusted by Adobe Photoshop as described above. The number of cells with nuclear Arc and cytoplasmice Arc ring was described as the percentage of all Arc-positive cells.

Confocal imaging. Representative images of Arc immunofluorescence were scanned using the Zeiss confocal microscope LSM 800 with a 63x oil immersion objective. The same scanning parameters were used for all samples. The images shown in Fig. 4 were chosen from a similar region of the motor cortex. Zen software from Zeiss was used to convert all confocal images into TIF images (RGB, 300 dpi). The contrast and brightness were uniformly adjusted using Adobe Photoshop.

Nuclear isolation. Nuclei were isolated from the frontal cortex using a combined version of the methods described by by Lovtrup-Rein et al. and Tanaka et al. (5, 6). All of the following processes were carried out at 4˚ C. The dissected frontal cortex was homogenized with A buffer [50 mM Tris-HCl (pH 7.5), 25 mM KCl, 5 mM $MgCl_2$, and 0.32 M sucrose] containing 0.25% Triton X-100, cOmplete™ mini (Roche), and a phosphatase inhibitor cocktail (Sigma-Aldrich) (sample 1) and centrifuged at 800 × *g* for 10 min,

subsequently, the supernatant (sample 2) was removed. The pellet was washed twice with the A buffer and centrifuged at 800 × *g* for 10 min. The pellet was resuspended in the A buffer, mixed with five volumes of sucrose buffer [50 mM Tris-HCl (pH 7.5), 25 mM KCl, 1 mM $CaCl_2$, 2.24 M sucrose, and 0.2% Nonidet-P], and centrifuged at 53,500 × *g* for 2 h. The pellet was used as the nuclear fraction (sample 3). All buffers mentioned above contained 1 mM PMSF. Fractionation was validated using sample 1–3 for total, cytoplasmic, and nuclear proteins, respectively, using Coomassie staining and immunoblotting (SI Appendix, Fig. S6C). For immunoblot analysis, nuclear samples were lysed in a 2D lysis buffer (7), while total homogenates and cytoplasmic samples were combined in the same volume of the 2D lysis buffer.

Statistics. Data were expressed as the mean and SEM. Immunoblotting and qRT–PCR data were expressed relative to the means of WT ZT4 control mice. Statistical analysis was performed using GraphPad Prism7. Once two-way ANOVA detects a significance ($P < 0.05$), Sidak's multiple comparison tests were subsequently performed. Student's unpaired *t*-test was carried out for comparisons between two groups.

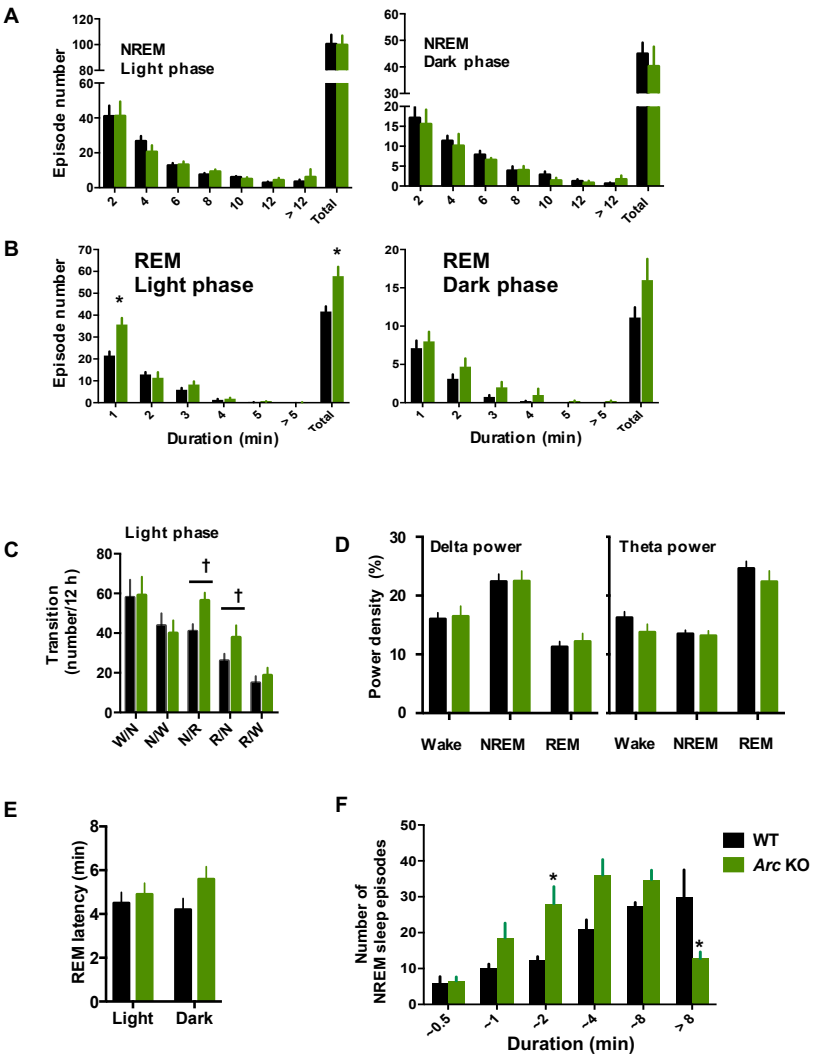

Fig. S1. *Arc* KO mice sleep phenotype and sleep parameters.

Panels A-E indicate baseline conditions, whereas panel F shows recovery condition (ZT4-24). (A, B) Distribution of the number of NREM (A) and REM (B) episodes in the light (left) and dark (right) phases. (B) *Arc* KO mice showed increases in short-duration (<1 min) and in the total number of REM episodes in the light phase compared to WT mice (F (1, 13) = 11.7, P = 0.005, two-way ANOVA). (C) Number of transitions between wakefulness (W), NREM sleep (N), and REM sleep (R) in the light phase. *Arc* KO mice showed a high frequency of transitions from NREM to REM (N/R) (P = 0.003, t-test) and REM to NREM (R/N) (P = 0.001, t-test) compared to WT mice. (D) Delta and theta power in wakefulness, NREM and REM sleep states. No significant differences were observed in delta (left) or theta (right) power across the conditions between the genotypes. (E) REM sleep latency was not significantly different between genotypes in the light (P = 0.51) and dark (P = 0.10) phases. (F) NREM sleep episode consolidation after 4-h SD. Values are expressed as means + SEM (n = 7 and 8 in each genotype). * P < 0.05 compared between genotypes by Sidak's multiple-comparisons test following two-way ANOVA; † P < 0.05 by unpaired Student's t-test between genotypes.

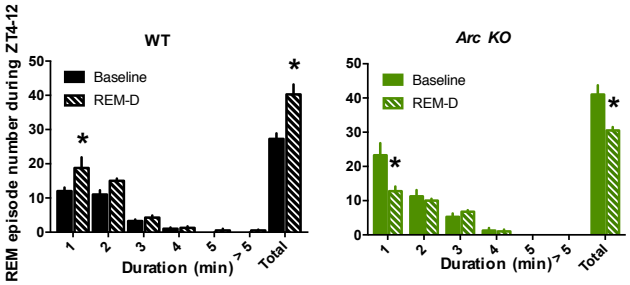

Fig. S2. Changes in REM episode duration after a selective 4-h REM deprivation

The distribution of the number of REM episodes was expressed as a 2-h bin during recovery (ZT4–12) following a 4-h selective REM deprivation (REM-D, ZT0–4) in WT (left) and *Arc* KO (right) mice. WT animals showed increases in short REM episode duration and total number of REM episodes (F (1, 3) = 37.6, P = 0.009, two-way ANOVA), while *Arc* KO mice showed significant decreases in these parameters (F (1, 3) = 17.2, P = 0.03, two-way ANOVA). * $P < 0.05$ compared with time-matched baseline by Sidak's multiple-comparisons test following two-way ANOVA (n = 4 in each genotype).

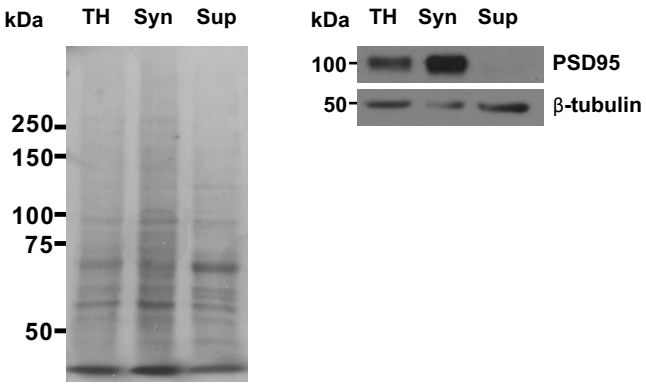

Fig. S3. Variation in synaptoneurosome isolation.

Left: Protein samples (10 μg each) were separated by 7.5% SDS–PAGE and transferred onto a PVDF membrane. The Coomassie-stained membrane shows a clear difference in the protein pattern among the total homogenate (TH), synaptoneurosome (Syn), and supernatant (Sup). *Right*: In the immunoblot, PSD95 (*top*) and β-tubulin (*bottom)* were used as synaptic and cytoplasmic markers, respectively. PSD95 was enriched and β-tubulin was diminished in Syn.

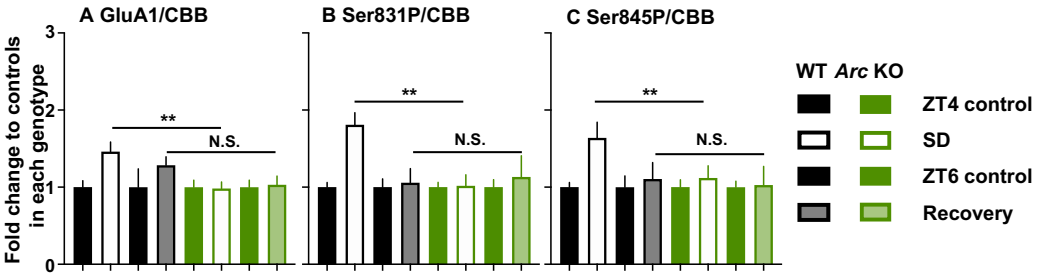

Fig. S4. Comparison of changes in SD-induced Synaptoneurosome GluA1 expression between genotypes. The results of Fig. 2C–E were re-normalized to its respective time-matched control at ZT4 or ZT6 and expressed as fold changes. Following 4-h SD, *Arc* KO mice showed significantly lower synaptoneurosome GluA1 (A), GluA1 phosphorylation at Ser831 (Ser831P, B), and Ser845 (Ser845P, C) levels than those of WT mice. Following 2-h recovery sleep, no significant differences were observed in GluA1, Ser831P, and Ser845P expression in synaptoneurosomes between the genotypes. ** P <0.01, N.S., not significant by Sidak's multiple-comparison test following two-way ANOVA between genotypes (n = 8–14 in each genotype).

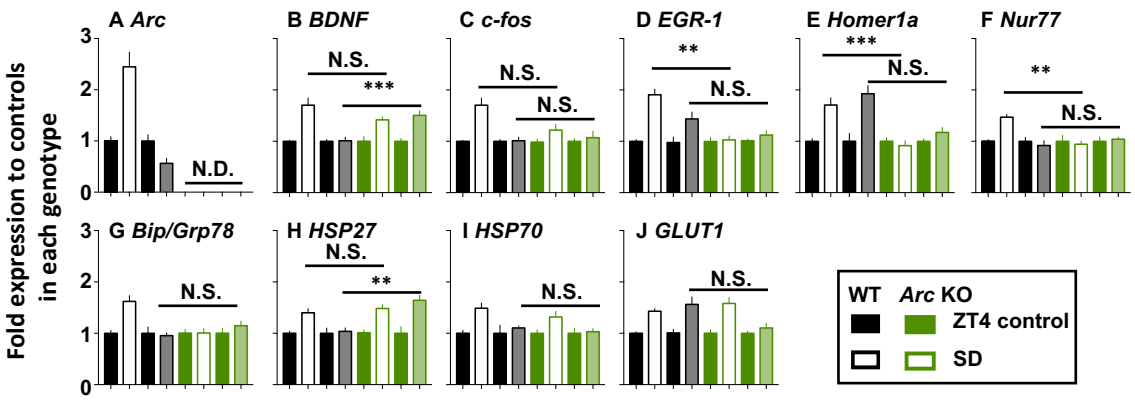

Fig. S5. Comparison of changes in seep-related gene expression in response to SD and recovery sleep between genotypes.

To compare SD-induced gene expression between the genotypes, the expression of the sleep-related genes shown in Fig. 3 was re-normalized to its time-matched control at ZT4 or ZT6, and expressed as fold change. After 4-h SD, Arc KO mice showed an attenuation of SD-induced *EGR-1* (D), *Homer1a* (E), *Nur77* (F), and *Bip/Grp78* (G) mRNA levels compared with WT mice. Following 2-h recovery sleep, *Arc* KO mice maintained higher levels of *BDNF* and *HSP27* mRNAs (B, I) compared to WT mice, suggesting that *Arc* KO mice lacked the ability to revert the levels of those genes to control compared to WT mice. No significant differences were observed in the other genes at ZT6 (A, C–G, I, J). These results were approximately consistent with the result from Figure 3. ** P <0.01, *** P <0.0001, N.S., not significant by Sidak's multiple-comparison test following two-way ANOVA; N.D., not detected (n = 6–14).

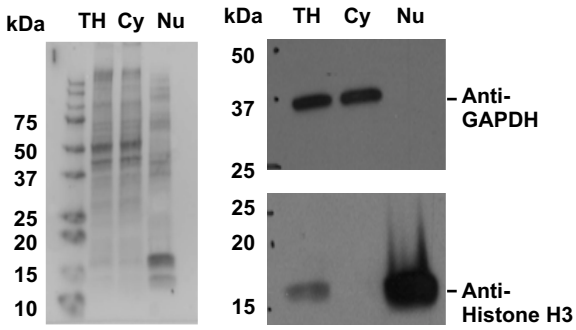

Fig. S6. Subcellular fractionations of nuclear and cytoplasm were verified by immune blot.

Variation in nuclear fraction isolation. *Left*: Protein samples (10 µg each) were separated by 12% SDS–PAGE and transferred onto a PVDF membrane. The Coomassie-stained membrane showed a clear difference in the protein pattern between the nuclear fraction (Nu) and total homogenate (TH) and/or cytoplasmic fraction (Cy). *Right*: In the immunoblot, GAPDH (right *top*) and histone H3 (right *bottom)* were used as cytoplasmic and nuclear protein markers, respectively. The nuclear protein was enriched in Nu, which showed hardly detectable GAPDH (*right top*) and robust histone H3 (*right bottom*) signals relative to the TH and Cy samples.

Table S1. Sequences of primer pairs for real-time quantitative PCR (qRT-PCR)

Gene	Forward/Reverse	Sequence	Accession no.
Arc	Forward	Mm01204954_g1 (Taqman probe)	NM_018790.3
	Reverse		
BDNF	Forward	CCATAAAGGACGCGGACTTGTACA	NM_007540.4
	Reverse	AGACATGTTTGCGGCATCCAG	
Bip/GRP78	Forward	GCTTCGTGTCTCCTCCTGAC	NM_022310.3
	Reverse	GGAATAGGTGGTCCCCAAGT	
c-fos	Forward	CTGTCAACACACAGGACTTTT	NM_010234.2
	Reverse	AGGAGATAGCTGCTCTACTTTG	
EGR-1	Forward	GCCGAGCGAACAACCCTA	NM_007913
	Reverse	TTCAGAGCGATGTCAGAAA	
GAPDH	Forward	GTGGCAAAGTGGAGATTGTTGCC	NM_008084.3
	Reverse	GATGATGACCCGTTTGGCTCC	
GluA1	Forward	Mm00433753_m1 (Taqman probe)	NM_001113325.2
	Reverse		
GLUT1	Forward	CCTATGGCCAAGGACACACT	NM_011400.3
	Reverse	CTGGTGTCAGGCAAGGAAAG	
HSP27	Forward	GACAGCTCAGCAGCGGGGTCTC	NM_011982.2
	Reverse	TAAGTGTGCCCTCAGGGGATAGGG	
HSP70	Forward	CCAAGGTGCAGGTGAACTACA	NM_031165.4
	Reverse	TCAGCACCATGGACGAGATCT	
Homer1a	Forward	ATGAACTTCCATATTTATCCACCTTACTT	NM_013560.2
	Reverse	GCATTGCCATTTCCACATAGG	
Nur77	Forward	TGATGTTCCCGCCTTTGC	NM_010444.1
	Reverse	GAGCCCGTGTCGATCAGTG	

Arc, activity-regulated cytoskeletal-associated protein; *BDNF*, brain-derived neurotrophic factor; *Bip/GRP78*, binding immunoglobulin protein/glucose-regulated protein 78; *EGR-1*, early growth response protein 1; *GAPDH*, glyceraldehyde 3-phosphate dehydrogenase; *GluA1*, α-amino-3-hydroxy-5-methyl-4-isoxazolepropionic acid (AMPA) receptor, glutamate A1; *Glut1*, glucose transporter 1; *HSP27*, heat shock protein 27; *HSP70*, heat shock protein 70

SI References

1. Wang KH, et al. (2006) In vivo two-photon imaging reveals a role of arc in enhancing orientation specificity in visual cortex. *Cell* 126(2):389–402.
2. Bjorness TE, Kelly CL, Gao T, Poffenberger V, Greene RW (2009) Control and Function of the Homeostatic Sleep Response by Adenosine A1 Receptors. *J Neurosci* 29(5):1267–1276.
3. Bermejo MK, Milenkovic M, Salahpour A, Ramsey AJ (2014) Preparation of Synaptic Plasma Membrane and Postsynaptic Density Proteins Using a Discontinuous Sucrose Gradient. *J Vis Exp* (91):1–8.
4. Vyazovskiy V V., Cirelli C, Pfister-Genskow M, Faraguna U, Tononi G (2008) Molecular and electrophysiological evidence for net synaptic potentiation in wake and depression in sleep. *Nat Neurosci* 11(2):200–208.
5. Lovtrup-Rein H, McEwen BS (1966) Isolation and fractionation of rat brain nuclei. J Cell Biol 30(2):405–415.
6. Tanaka T, Kishi K, Igawa M, Takase S, Goda T (1998) Dietary carbohydrates enhance lactase/phlorizin hydrolase gene expression at a transcription level in rat jejunum. *Biochem J* 331(1):225–230.
7. Suzuki A, Sinton CM, Greene RW, Yanagisawa M (2013) Behavioral and biochemical dissociation of arousal and homeostatic sleep need influenced by prior wakeful experience in mice. *Proc Natl Acad Sci* 110(25):10288–10293.